Molecular Crystals and Liquid Crystals

Publication details, including instructions for authors and subscription information:
http://www.tandfonline.com/loi/gmcl20

Discotic Mesogen - DNA Complex Films at Interfaces

K. A. Suresh [a] & Alpana Nayak [b]

[a] Centre for Liquid Crystal Research, Jalahalli, Bangalore, India

[b] Raman Research Institute, Sadashivanagar, Bangalore, India

Version of record first published: 05 Oct 2009

To cite this article: K. A. Suresh & Alpana Nayak (2009): Discotic Mesogen - DNA Complex Films at Interfaces, Molecular Crystals and Liquid Crystals, 512:1, 57/[1903]-80/[1926]

To link to this article: http://dx.doi.org/10.1080/15421400903050459

Mol. Cryst. Liq. Cryst., Vol. 512, pp. 57/[1903]–80/[1926], 2009

ISSN: 1542-1406 print/1563-5287 online
DOI: 10.1080/15421400903050459

Discotic Mesogen – DNA Complex Films at Interfaces

K. A. Suresh[1] and Alpana Nayak[2]
[1]Centre for Liquid Crystal Research, Jalahalli, Bangalore, India
[2]Raman Research Institute, Sadashivanagar, Bangalore, India

In this article, we review our studies on discotic mesogen – DNA complex films at interfaces. Discotic molecules are known to form highly anisotropic structures at the air-water (A-W) interface. We have studied films of a novel ionic discotic mesogenic molecule, pyridinium salt tethered with hexaalkoxytriphenylene (PyTp) and its complex with DNA (PyTp-DNA) at A-W and air-solid interfaces. The PyTp monolayer was formed on the aqueous subphase containing small amount of DNA. The electrostatic interaction between PyTp and DNA molecules results in a PyTp-DNA complex monolayer. Compared to the pure PyTp monolayer, the PyTp-DNA complex monolayer exhibits higher collapse pressure and lower limiting area. Surface manometry and Brewster angle microscope studies of the PyTp-DNA complex monolayer film indicate the molecules to be in the edge-on configuration. With increase in surface pressure, the complex monolayer undergoes a transition from a loosely packed monolayer phase to a compactly packed monolayer phase. The PyTp-DNA complex films on silicon wafers were prepared using Langmuir-Blodgett (LB) technique. We find that several tens of layers of PyTp-DNA complex monolayer can be transferred with good efficiency. We have carried out nanoscale electrical conductivity measurements for the pure PyTp and PyTp-DNA complex LB films using current sensing atomic force microscope. We have studied the current-voltage (I-V) characteristics for the metal-LB film-metal junction and our analysis shows that the I-V curves followed the Fowler-Nordheim tunneling model.

Keywords: current-sensing AFM; Langmuir-Blodgett films; mesogen – DNA complex; nanoscale electrical conductivity

We are thankful to Santanu Kumar Pal and Sandeep Kumar for providing us the material, pyridinium salt tethered with hexaalkoxytriphenylene (PyTp) for our experiments.

Address correspondence to K. A. Suresh, Centre for Liquid Crystal Research, P.B. No. 1329, Jalahalli, Bangalore 560013, India. E-mail: suresh@clcr.res.in

I. INTRODUCTION

The thin films of discotic mesogenic molecules (discogens) have technological applications in the fabrication of gas sensors, field-effect transistors, photovoltaic solar cells and light emitting diodes [1]. As compared to the conventional discogens, ionic discogens differ significantly as they combine the properties of liquid crystals and ionic liquids. This makes them promising candidates to design anisotropic ion conductive materials because of the anisotropic structural organization and the presence of ions as charge carriers [2]. Discotic molecules can self-assemble into one-dimensional columnar superstructures due to the overlapping of the Π-orbitals of adjacent molecules and can arrange in a two-dimensional lattice at the air–water (A-W) interface, thereby forming stable Langmuir monolayers [3]. These thin films need to be transferred to solid supports for practical applications, and employing Langmuir-Blodgett (LB) technique is an efficient method to obtain highly ordered layers over large areas [4].

In recent years, the interaction of DNA with molecules in a monolayer at A-W interface has received considerable attention, with a view to understand templated supramolecular organization as well as the transfer of DNA across biological bilayer membranes [5–7]. A variety of cationic surfactants, such as linear and branched polymer, glycopeptides, and dendrimers, as well as lipid membranes, have been shown to be capable of complexing with DNA [8,9]. Langmuir-Blodgett (LB) films are useful for immobilization of nucleic acids (DNA, polynucleotides) on solid supports in the designing of nucleic acid-based biosensors [10]. The immobilization of DNA molecules on a solid substrate by means of electrostatic interactions has a clear advantage, as compared with chemical bonding. Although there have been many studies on the formation of DNA-cationic lipid complexes, there have been no reports on the interaction of DNA with cationic discotic molecules at the A-W interface. Recently, Cui et al. reported DNA complexes with cationic discotic surfactants in the bulk [11]. The interaction of DNA with a discotic surfactant in the bulk is different from such an interaction at the A-W interface.

Discotic mesogenic molecules possess unique molecular electronic properties, like two-dimensional delocalizations of electrons, which are not observed in linear oligomers and polymers [12]. In addition, these molecular electronic properties are amplified at the supramolecular level due to the extended interactions between Π-systems. Therefore, discogens are a truly new generation of organic semiconductors [1]. In addition, the DNA molecule has drawn lot of attention in nanoelectronic devices due to its intrinsic electronic properties. The

charge-transfer reactions and conductivity measurements show a large variety of possible electronic behavior [13]. Since both DNA and discogens have their own intrinsic electronic properties, complexing DNA with cationic discogen molecules is a novel approach for developing advanced materials with interesting electronic properties. To study electron conduction at molecular level, scanning probe techniques (scanning tunneling microscope (STM) and current sensing atomic force microscope (CS-AFM)) are the most suitable methods [14,15]. CS-AFM provides an attractive approach to electrically contacting monolayer films under controlled load and the formation of metal-molecule-metal junction. Additionally, in CS-AFM, the images of topography and current are simultaneously obtained, enabling direct correlation of local topography with electrical properties at nanoscale. The conventional CS-AFM operates in contact mode. For soft systems, the damage due to lateral shear forces in contact mode imaging is an important issue. However, for systems like self assembled monolayer and polymers, the contact mode can still be used [16].

In this article, we review our studies on the films of a cationic discogen, pyridinium salt tethered with hexaalkoxytriphenylene (PyTp) and its complex with DNA (PyTp-DNA) at both A-W and air-solid (A-S) interfaces [17,18]. We find that, at A-W interface, the PyTp-DNA complex monolayer exhibits a higher collapse pressure, compared to the pure PyTp monolayer, indicating better stability. Using LB technique, we have transferred these films onto solid substrates. We find that the formation of the DNA complex enhanced the transfer efficiency over several tens of layers. The efficiency of the PyTp-DNA complex to form multilayers on a substrate can find application in devices such as thin film transistors and nucleic acid based biosensors [10,19]. Our AFM studies show that the PyTp-DNA complex films transferred onto silicon wafers are quite compact. In addition, the electrical conductivity measurements at nanoscale were performed on the LB films of both pure PyTp and PyTp-DNA complex employing CS-AFM. Our measurements show that the conductivity of PyTp-DNA complex film is much less compared to the pure PyTp film [20]. The ability to rationally design molecular electronic components hinges on a fundamental understanding of the charge transport mechanism in metal-molecule-metal junctions. To this end, we look for a possible mechanism for electron transport at nanoscale in such a system. The analysis of the current-voltage (I-V) curves suggests that the electron transport mechanism in our system follows the Fowler-Nordheim tunneling model.

II. EXPERIMENT

The material PyTp was synthesized by Sandeep Kumar and Santanu K. Pal [21]. The thermotropic liquid crystalline properties of this material were investigated by polarizing optical microscopy and differential scanning calorimetry.

The surface manometry experiments were carried out using a NIMA 611 M trough. The subphase used was ultrapure deionized water (pH 5.8) obtained from Millipore Milli-Q system. The surface pressure (π)-area per molecule (A_m) isotherms were obtained by symmetric compression of the barriers with a constant compression rate of 0.103 nm^2/molecule/min. The surface pressure (π) was measured using the standard Wilhelmy plate technique. For complexation with DNA, sodium salt of DNA (Sigma) was dissolved in the ultrapure water subphase. This is a double-stranded DNA from Salmon testes with approximate molecular weight of 1.3×10^6 ($\sim$2000 bp). The π-A_m isotherm for the complex monolayer was obtained by spreading the stock solution of PyTp on the subphase containing DNA at various concentrations. A Brewster angle microscope (BAM), MiniBAM (NFT, Nanotech, Germany) was employed to observe the films at the A-W interface. LB technique was employed to transfer various layers of the films onto hydrophilic and hydrophobic substrates at different target surface pressures (π_t) with a dipping speed of 2 mm/min. To obtain hydrophilic surfaces, the polished silicon wafers were treated for about 5 min in hot piranha solution (mixture of concentrated H_2SO_4 and H_2O_2 in 3:1 ratio) which were then rinsed in ultrapure deionized water and later dried. For hydrophobic surfaces, clean silicon substrates were dipped in hexamethyldisilazane (HMDS) for 12 hours and then rinsed with HPLC grade chloroform. Horizontal transfer technique was used to obtain films on substrates at low π.

The atomic force microscope (AFM) studies on these LB films were performed using model PicoPlus (Molecular Imaging). The topography of the films were obtained in the AC mode AFM using silicon tips with spring constant of 21 N/m and resonance frequency 250 kHz (Nanosensors, USA). To obtain the thickness, the films were scratched with the same tip in contact mode. The topography of the scratched region was imaged in the AC mode.

For electrical conductivity measurements, we have formed the films on gold coated mica substrate. These substrates were very clean and hence just rinsed with HPLC grade chloroform before film deposition. The conductivity measurements were carried out using a contact mode CS-AFM. We have used platinum coated silicon cantilevers having spring constant in the range of 0.02 to 0.8 N/m, tip radius $\sim$30 nm

and resonance frequency in the range of 5 to 25 kHz for CS-AFM measurements. The conductive tip behaves effectively as a metal electrode with an area mainly determined by the tip-sample contact region. With the tip at virtual ground, a selectable bias voltage was applied between the tip and sample. A preamplifier, with a sensitivity of 1 nA/Volt and operational range from 1 pA to 10 nA was used. In our CS-AFM apparatus, the rms noise level was 2 pA and hence any signal above this was detectable. The deflection of the cantilever was monitored and kept constant to maintain a constant force between the tip and sample, and simultaneous topographic and current images were generated. During I-V measurements, the feedback loop was enabled, meaning that the force applied by the cantilever was held constant. In addition, after every I-V measurements, we have scanned the same region of the film to confirm that the film was not damaged.

III. RESULTS AND DISCUSSION

The material PyTp exhibits the following liquid crystal phase sequence: solid (S) – columnar phase (Col); 83.7°C, Col – isotropic; 95°C. On cooling, the columnar mesophase appeared at 92°C and remained stable down to room temperature [20].

Surface Manometry

The π-A_m isotherms for the PyTp molecule with different molar concentrations of DNA in the subphase are shown in Figure 1. The isotherm for pure PyTp (which is formed on ultra pure deionized water subphase) shows a gradual rise in π up to 9 mN/m followed by a sharp rise and finally collapses at a π of about 44 mN/m. The limiting area per molecule (A_o) values obtained by extrapolation to zero surface pressure were 1.15 nm^2/molecule at the steep increasing region and 3.1 nm^2/molecule at the gradual increasing region respectively. Figure 2 shows the molecular structure of PyTp according to standard bond lengths and angles. The computed surface area of the aromatic core is equal to 0.785 nm^2. The surface area occupied by the molecule increases to 4.5 nm^2 if the extended peripheral hydrocarbon tails are included. The observed A_o values for the first transformation suggest an expanded phase, whereas for the second transformation, the observed A_o values suggest a condensed phase. The nature of the isotherm of the PyTp monolayer changes with the addition of DNA in the subphase. We find that, the collapse pressure increases and the A_o value of the isotherm decreases with the increase in the concentration of DNA in the subphase.

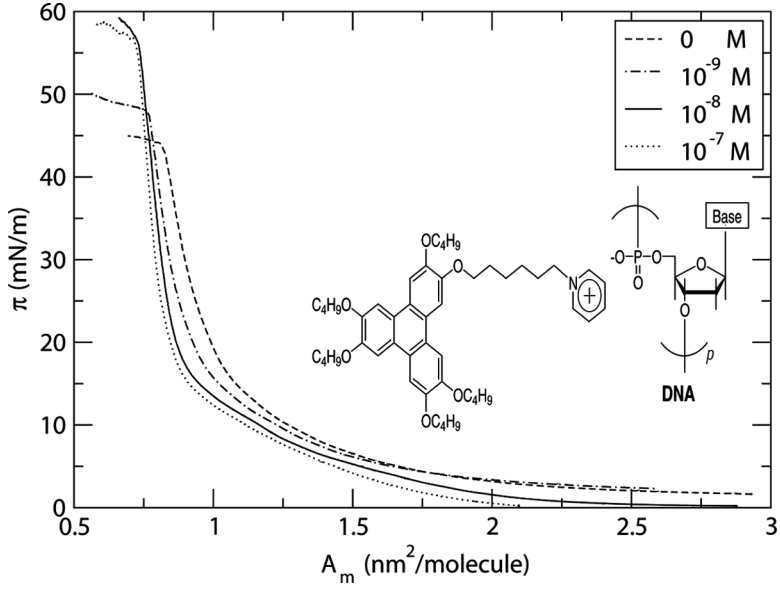

FIGURE 1 Surface pressure (π)-area per molecule (A_m) isotherms for the monolayer of PyTp-DNA complex for different concentrations of DNA in the subphase. Reprinted with permission from reference 18. Copyright 2008 American Chemical Society.

However, beyond 10^{-8} M concentration of DNA, there was no further change in the isotherm. The decrease in the A_o value and the increase in the collapse pressure as compared to the pure PyTp monolyer indicates condensation and enhanced stability of the PyTp-DNA complex monolayer. For the 10^{-8} M concentration, the collapse pressure was about 58 mN/m, which is 25% higher as compared to the pure PyTp monolayer. The isotherm exhibited a clear slope change at 0.95 nm^2/molecule, indicating a phase transformation. The A_o value was 1.9 nm^2/molecule for the first transformation and 0.9 nm^2/molecule for the second transformation. Comparing with the molecular dimension, we suggest that the molecules adopt the edge-on conformation with a value of 1.9 nm^2/molecule, corresponding to an expanded phase, and a value of 0.9 nm^2/molecule, corresponding to a condensed phase. In addition, the isotherm cycles performed by compression and expansion of the PyTp-DNA complex monolayer at the condensed phase showed a negligible amount of hysteresis. However, if the isotherm cycles were performed after the complex monolayer reached the collapsed state, an appreciable amount of hysteresis was observed,

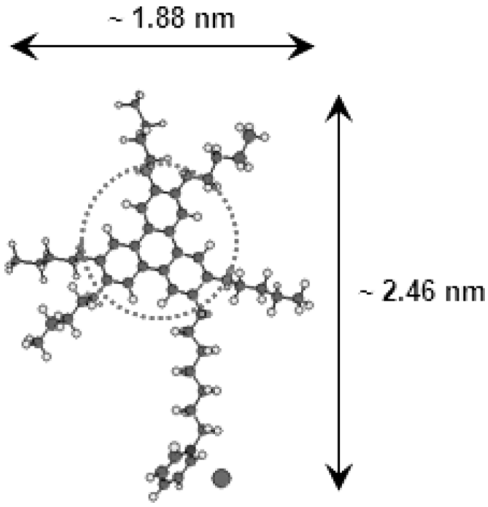

FIGURE 2 Molecular structure of PyTp according to the standard bond lengths and angles. The triphenylene disc area shown in dotted circle is about $0.785\,nm^2$.

and the monolayer did not exhibit reversibility on expansion. This behavior was unlike the pure PyTp monolayer, which showed completely reversible collapse. This indicated a stable complex formation between DNA and the cationic PyTp molecules at the A-W interface.

The rigidity of the films were calculated from the compressional elastic modulus, |E| given by $|E| = A_m(d\pi/dA_m)$. The |E| value characterizes the nature of a monolayer's stable phases [22]. Specifically, a maximum value of the |E| in the range of 12.5 mN/m to 50 mN/m is characteristic of liquid expanded phase, whereas a value between 100 and 250 mN/m is characteristic of the liquid condensed phase [23]. The variation of |E| with A_m obtained from the isotherms of pure PyTp monolayer and PyTp-DNA complex monolayer are shown in Figure 3. The variation of |E| with A_m showed a maximum of 83 mN/m at A_m of $0.871\,nm^2$/molecule for the pure PyTp monolayer, whereas, the |E| value showed a maximum of 283 mN/m at an A_m of $0.78\,nm^2$/molecule for the PyTp-DNA complex monolayer. Interestingly, the maximum |E| value attained by the complex monolayer was more than three times the value attained by the pure PyTp monolayer, indicating a much better packing of molecules in the complex monolayer as compared to that of a pure PyTp monolayer. We find a sharp change in the value of |E| at an A_m of $0.95\,nm^2$/molecule for the complex monolayer, indicating a phase transition. The phase above an A_m of

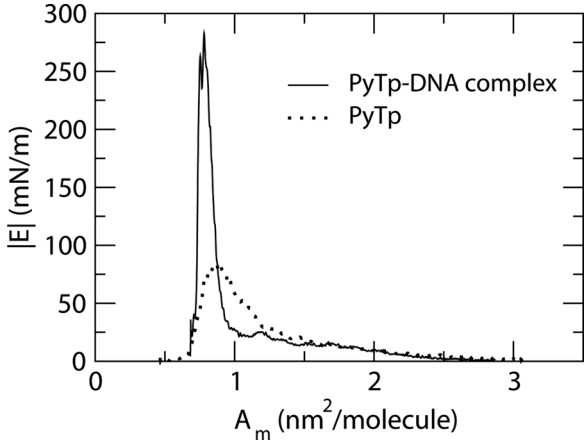

FIGURE 3 Variation of compressional elastic modulus (|E|) with area per molecule (A_m) for the pure PyTp monolayer (dotted line) and the PyTp-DNA complex monolayer (continuous line) with a 10^{-8} M concentration of DNA in the subphase. Reprinted with permission from reference 18. Copyright 2008 American Chemical Society.

$0.95\,nm^2$/molecule has a much lower value of |E| as compared to the phase below this A_m. This suggests that the complex monolayer undergoes a phase transition in the edge-on configuration from an expanded phase to a condensed phase.

Brewster Angle Microscopy

The BAM images of PyTp monolayer show that the brightness increases gradually upon compression from nearly zero surface pressure (Fig. 4a). This transforms to 3D crystals (Fig. 4b) at the collapsed state. On expansion, these crystalline domains disappeared, and the PyTp system reverted back to the uniform intensity region indicating a monolayer state. This observation confirms the reversibility of the PyTp film. The BAM images of the PyTp-DNA complex monolayer with 10^{-8} M concentration of DNA in the subphase are shown in Figure 5. Similar to the pure PyTp monolayer, the intensity in the BAM image of the PyTp-DNA complex film increases gradually upon compression (Fig. 5a). But in the collapsed state, the 3D domains were markedly different. Pure PyTp film showed small crystalline domains filling the whole surface of water in a mesh-like texture. On the contrary, the PyTp-DNA complex film showed long, thread-like 3D crystals (Fig. 5b) at collapse. On expansion, these thread-like domains

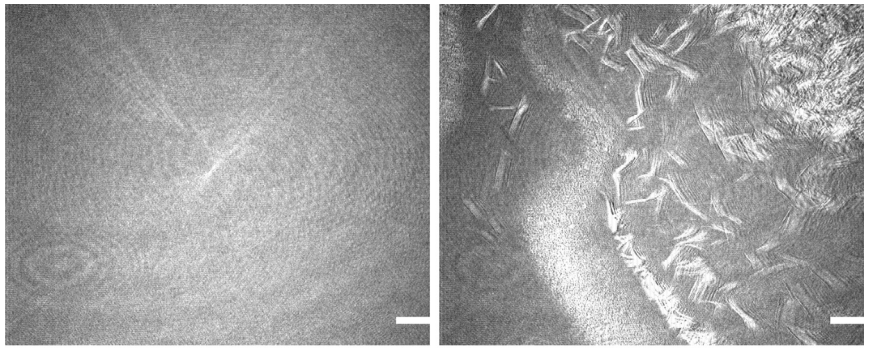

(a) (b)

FIGURE 4 BAM images of PyTp. (a) Condensed phase ($A_m = 1.2\,nm^2$), (b) collapsed state ($A_m = 0.7\,nm^2$); coexistence of 3D crystals and condensed phase. The scale bar in each image represents 500 μm. Reprinted with permission from reference 17. Copyright 2007 American Chemical Society.

continued without change, and the PyTp-DNA complex monolayer did not revert back to its original state. These results, together with surface manometry, indicated the stable complex formation between the DNA molecules and the cationic discotic PyTp molecules at the A-W interface. Here, the interaction is mainly electrostatic between the pyridinium group of discotic mesogen and the phosphate group of DNA, which play an important role in the formation and stability of the complex films.

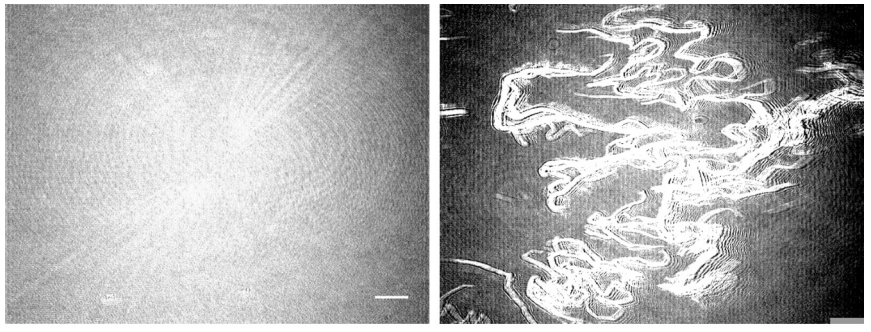

(a) (b)

FIGURE 5 BAM images of PyTp-DNA complex monolayer at (a) $A_m = 0.85\,nm^2$ and (b) $A_m = 0.35\,nm^2$, for DNA concentration of 10^{-8} M in the subphase. The scale bar in each image represents 500 μm. Reprinted with permission from reference 18. Copyright 2008 American Chemical Society.

Atomic Force Microscopy

Topography

The AFM topography images of the PyTp monolayer transferred at expanded phase (5 mN/m) by horizontal method on a hydrophilic silicon substrate (Fig. 6a) shows the height of the film to be about 0.7 nm with reference to the substrate. This corresponds to the thickness of the molecules lying parallel to the A-S interface. When the monolayer was transferred at the condensed phase (35 mN/m) by LB technique (Fig. 6b), the topography shows a uniform and homogeneous film with a height of about 2 nm with reference to the substrate. This corresponds to the thickness of the molecules lying normal to the A-S interface.

The π-A_m isotherm of PyTp and its |E| values indicate a phase transformation from an expanded phase to a condensed phase. The A_o values obtained in the expanded phase was 3.1 nm^2/molecule and in the condensed phase was 1.15 nm^2/molecule. Also, the AFM topography images showed a height of about 0.7 nm for the PyTp film transferred at expanded phase and a height of about 2 nm for the PyTp film

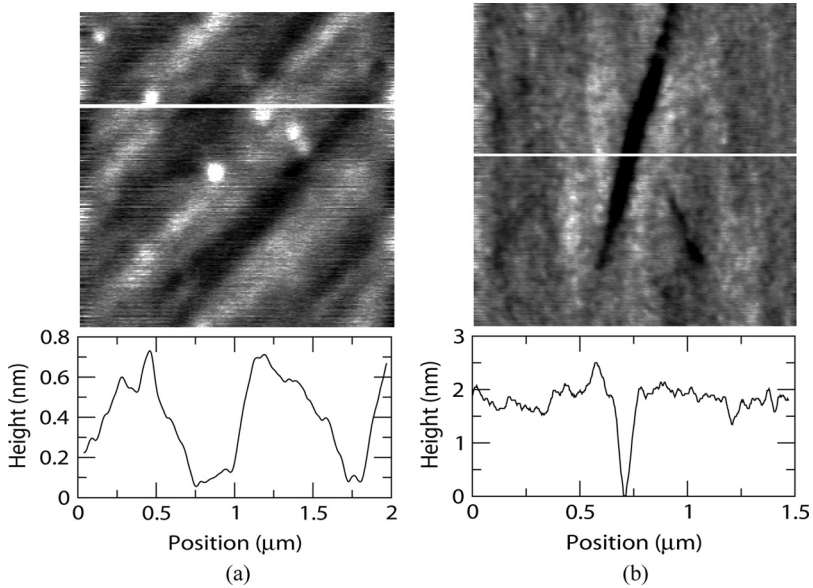

FIGURE 6 The AFM images of PyTp monolayer transferred onto hydrophilic silicon substrates at target surface pressures; (a) $\pi_t = 5$ mN/m, (b) $\pi_t = 35$ mN/m. The respective height profiles corresponding to the white line on the images are shown below.

transferred at condensed phase. Comparing all these results with the molecular dimensions (Fig. 2), we infer the molecules to have a face-on structure at the expanded phase and an edge-on structure at the condensed phase. This also indicates that the structure of the Langmuir films was maintained throughout the transfer process from the A-W interface to the A-S interface. On the basis of these results, we represent the face-on and edge-on configuration at the A-W interface as shown in Figure 7.

In face-on configuration, the core lies flat on the water surface and the hydrocarbon tails (partially interdigited) extend away from the interface. Such a configuration may be preferred if the core of the molecule is capable of hydrogen bonding. It also maximizes the configuration space available to the aliphatic tails. In the edge-on configuration the core lies normal to the interface with the polar end submerged in the water and bottom most tails extending roughly parallel and slightly away from the interface. Such a state allows the polar oxygen to be in contact with water, while minimizing water contact with the hydrophobic alkyl tails. This maximizes the $\Pi-\Pi$ interactions between the conjugated cores with the molecules arranged into columns parallel to the water surface, forming the 2D analogue of a columnar phase. Josefowicz et al. have reported the edge-on columnar structure in the LB films of triphenylene-based discotic molecules with the column alignment predominantly along the film deposition direction [3]. However, they did not report face-on arrangement based on AFM. In our system, the presence of highly polar pyridinium moiety together with six oxygen atoms at the periphery of the triphenylene core have enhanced the hydrophilicity of the molecules, thereby facilitating the face-on configuration at large A_m values at the A-W interface.

The AFM image of the LB film of PyTp with two layers transferred onto hydrophobic silicon substrates at π_t of 35 mN/m (Fig. 8) revealed a

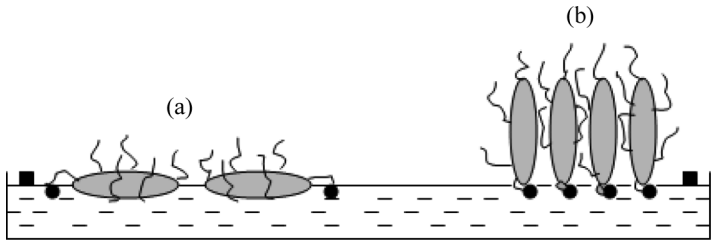

FIGURE 7 Schematic representation of the molecules in (a) face-on and (b) edge-on states at the A-W interface. Reprinted with permission from reference 17. Copyright 2007 American Chemical Society.

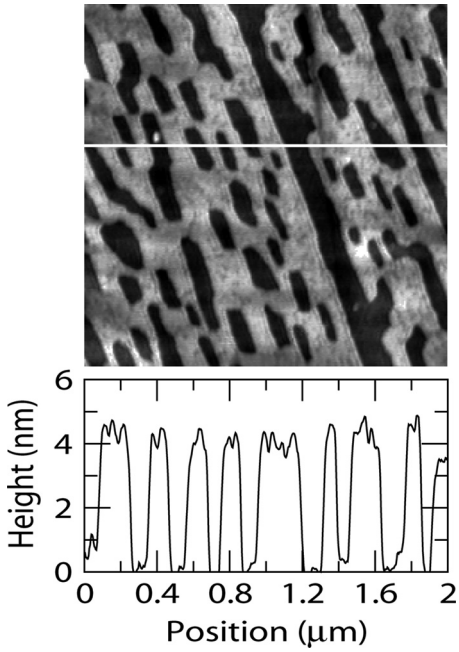

FIGURE 8 AFM image of PyTp film with two layers on hydrophobic silicon substrate at π_t of 35 mN/m. The height profile corresponding to the white line on the image is shown below. Reprinted with permission from reference 17. Copyright 2007 American Chemical Society.

morphology with narrow rectangular voids elongated in the film deposition direction. The height profile yields a value of about 4.2 nm. This corresponds to the value of two layers of the molecules in the edge-on configuration. The AFM images of the PyTp-DNA complex monolayer transferred onto hydrophilic silicon substrates are shown in Figure 9. The film transferred at a π_t of 5 mN/m (Fig. 9a) showed a height of 1.4 ± 0.4 nm with reference to the substrate. Comparing with the molecular dimension, this value lies between the values expected for a face-on and an edge-on configuration of molecules in the film.

The film morphology depicts the heterogeneity with streak-like features (length 200–300 nm, breadth 20–30 nm). These may be due to the DNA strands complexed with the PyTp molecules in the film. The morphology of the film transferred at a π_t of 35 mN/m (Fig. 9b) was compact and homogeneous with some small voids. The film showed a height of 3 ± 0.2 nm, which is more than the film height of

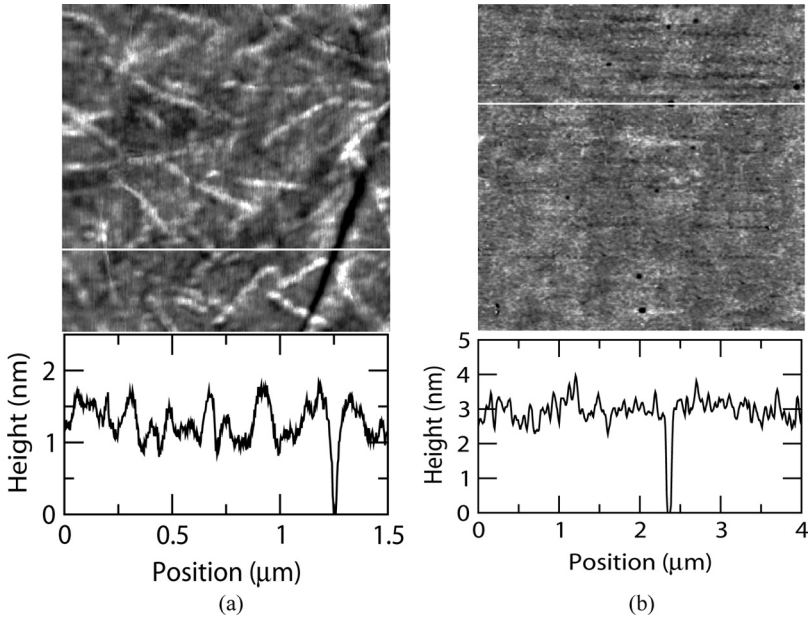

FIGURE 9 AFM images of a monolayer of the PyTp-DNA complex film transferred at (a) $\pi_t = 5\,mN/m$ and (b) $\pi_t = 35\,mN/m$ onto hydrophilic silicon substrates. The respective height profiles corresponding to the white lines on the images are shown below. Reprinted with permission from reference 18. Copyright 2008 American Chemical Society.

pure PyTp in the edge-on configuration by nearly 1 nm. This extra thickness of 1 nm can be attributed to the presence of DNA in the film. The π-A_m isotherm and the calculated |E| values indicated a phase transformation from an expanded phase to a condensed phase. The A_o value obtained in the expanded phase was $1.9\,nm^2$/molecule and in the condensed phase was $0.9\,nm^2$/molecule. Additionally, the AFM topography images showed a height of $\sim$1.4 nm for the film transferred at expanded phase and a height of $\sim$3 nm for the film transferred at condensed phase. Comparing all these results with the molecular dimension, we infer that the face-on configuration was suppressed. The phase transition was from loosely packed molecules in the edge-on configuration to a compactly packed edge-on configuration. On the basis of these results, we have drawn the configuration of molecules at the A-W interface in Figure 10.

Figure 11 represents AFM topography for two layers of the PyTp-DNA complex LB film deposited at 35 mN/m on a hydrophobic

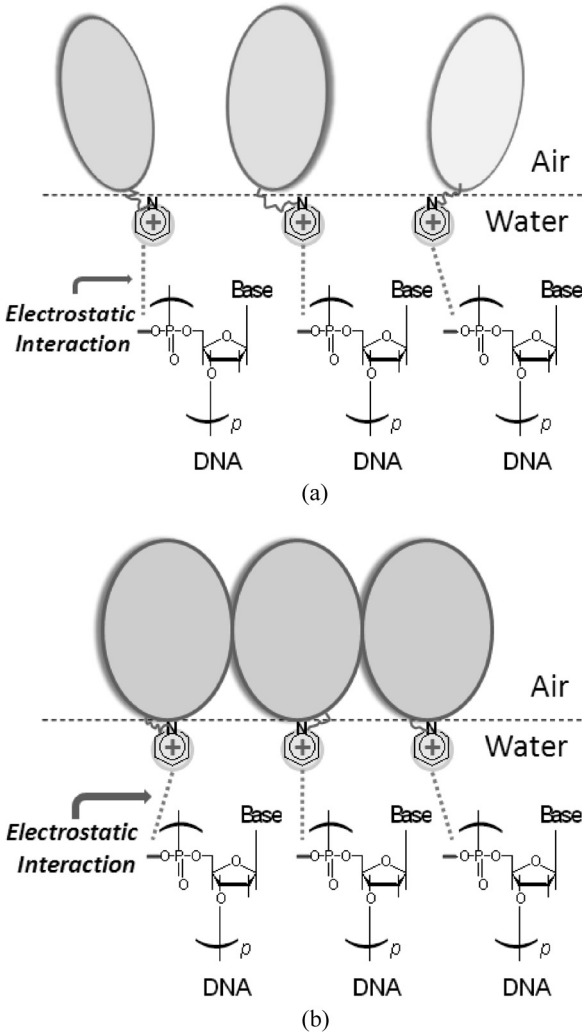

FIGURE 10 PyTp-DNA complex monolayer shown schematically in the edge-on configuration formed at the A-W interface. (a) Loosely packed molecules ($A_o = 1.9\,nm^2$/molecule). (b) Compactly packed molecules ($A_o = 0.9\,nm^2$/molecule). Reprinted with permission from reference 18. Copyright 2008 American Chemical Society.

silicon substrate. As compared to the two layers of pure PyTp film which had regular rectangular voids, the morphology of the PyTp-DNA complex film with two layers was more compact, with some

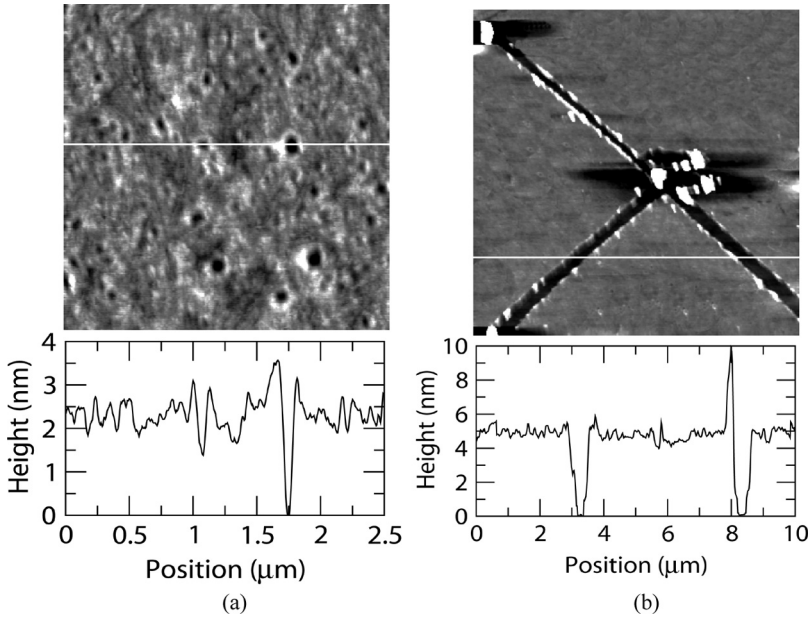

FIGURE 11 The AFM images for two layers of a PyTp-DNA complex film transferred at 35 mN/m onto hydrophobic silicon substrate. (a) Film surface showing circular voids. (b) Film surface showing the scratches to measure the thickness. The respective height profiles corresponding to the white lines on the images are shown below. Reprinted with permission from reference 18. Copyright 2008 American Chemical Society.

circular voids (Fig. 11a) of different depth. These voids might have developed in the film deposition process due to the drainage or evaporation of the entrapped water molecules within the films. To obtain the actual film thickness, we have scratched the film using an AFM tip in contact mode and then imaged the scratched region in tapping mode using the same tip (Fig. 11b). The film was scratched in different directions to obtain the correct thickness of the film with better reproducibility. The thickness of the film obtained by height profile across the scratch was 5 ± 0.5 nm. We have studied the morphology and thickness of the complex films transferred up to 20 layers. Scratching using the AFM tips became difficult for higher layers because of a large accumulation of materials at the edges. For this reason, scratching was not performed for films with more than 20 layers, although it was possible to transfer even 50 layers with good efficiency. The morphology of the complex film with 20 layers (Fig. 12) showed thread-like structures

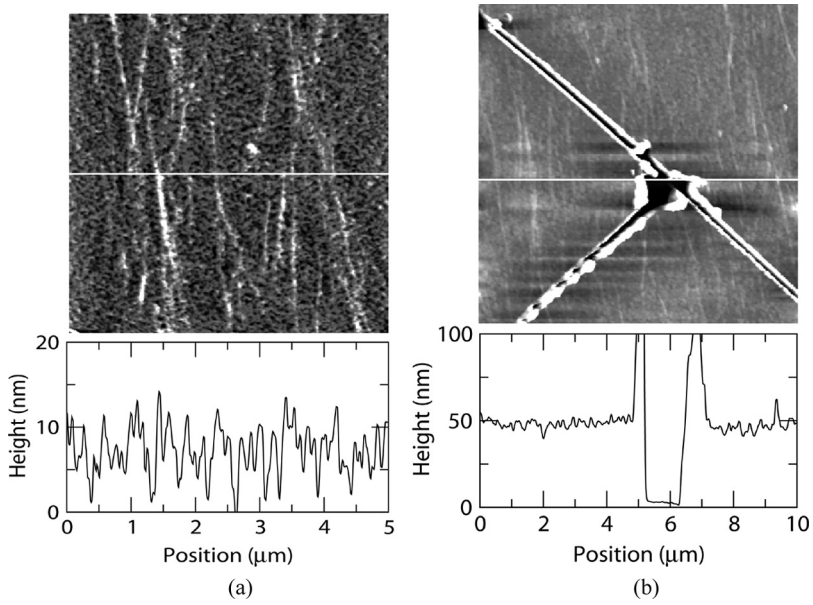

FIGURE 12 AFM topography images for 20 layers of PyTp-DNA complex film transferred at 35 mN/m onto hydrophobic silicon substrates. (a) Morphology of the film surface showing DNA bundles. (b) Scratched film to measure the thickness. The respective height profiles corresponding to the lines drawn on the images are shown below. Reprinted with permission from reference 18. Copyright 2008 American Chemical Society.

aligned in the film deposition direction. These thread-like structures appeared for films with more than five layers and grew in number with increasing layers. These may be attributed to DNA bundles. The strong $\Pi-\Pi$ stacking interaction between the discotic cores brings multiple DNA strands together forming these thread-like bundles. The typical dimensions of these bundles were $\sim$80 nm in width, 1.5–3.0 μm in length, and 10–12 nm in height. The notable variation in the dimensions of these DNA bundles suggests partial coiling up or self-folding of the DNA strands. Possible explanations for the alignment of these structures in the film deposition direction may be parallel alignment of the DNA strands at the A-W interface and an effect created as a result of the receding meniscus force during the transfer process. Our observation is consistent with the reports on the orientation of DNA strands along the dipping direction of LB films [5,24]. In the case of the pure PyTp film, it was not possible to transfer more than two layers efficiently. Interestingly, we find that the DNA

complexation facilitated the film deposition of several tens of layers with high transfer efficiency. The ability to transfer several layers gives an excellent scope for device applications such as transistors [19]. Moreover, immobilization of nucleic acids onto solid supports by the LB technique is a useful approach in designing nucleic acid based biosensors [10].

Current Images

For nanoscale electrical conductivity measurements, the PyTp monolayer film was deposited on gold coated mica substrate by LB technique. The films were imaged by contact mode CS-AFM. By maintaining a constant force of 4 nN between the tip and sample, simultaneous topographic and current images were obtained for sample bias voltages of 1 and 2 Volts. For the sample bias voltage of 1 Volt, a current flow in the range of 0.1 to 0.4 nA was observed. The current features were further resolved by increasing the sample bias to 2 Volts. The simultaneously acquired topography and current images for pure PyTp monolayer film at a bias voltage of 2 Volts are shown in Figures 13(a) and (b) respectively. At this bias voltage, a current flow of about 1 nA was observed across the film. The inhomogeneities observed in the current image might be due to the defects in the gold coating on mica substrate. Similar inhomogeneities were also observed for bare gold film coated on mica. Further, the probe works in contact mode in our methodology. The effects of contact forces are; slight compression of the film, changes in the contact area itself due to the film surface roughness. These are also possible reasons for current inhomogeneities. Such inhomogeneities in current images are also reported in literature for organic films [16]. The PyTp-DNA complex monolayer film formed on gold coated mica substrate was also imaged by CS-AFM. As compared to PyTp film, the PyTp-DNA complex film exhibited measurable conductivity only above 1 Volt sample bias.

I-V Spectroscopy

The I-V measurements were performed at various positions on both the pure and complex films formed on gold coated mica substrates. The I-V curves were acquired while the tip was held at a fixed position with a force of 4 nN and the applied voltage ramp was from -3 to $+3$ Volts with a scan rate of 1 Hz. The metal substrate, the film and the conducting tip form a nanoscopic metal-insulator-metal (M-I-M) junction as shown in Figure 14. Representative I-V curves on pure film and complex film are shown in Figures 15(a) and (b) respectively. The

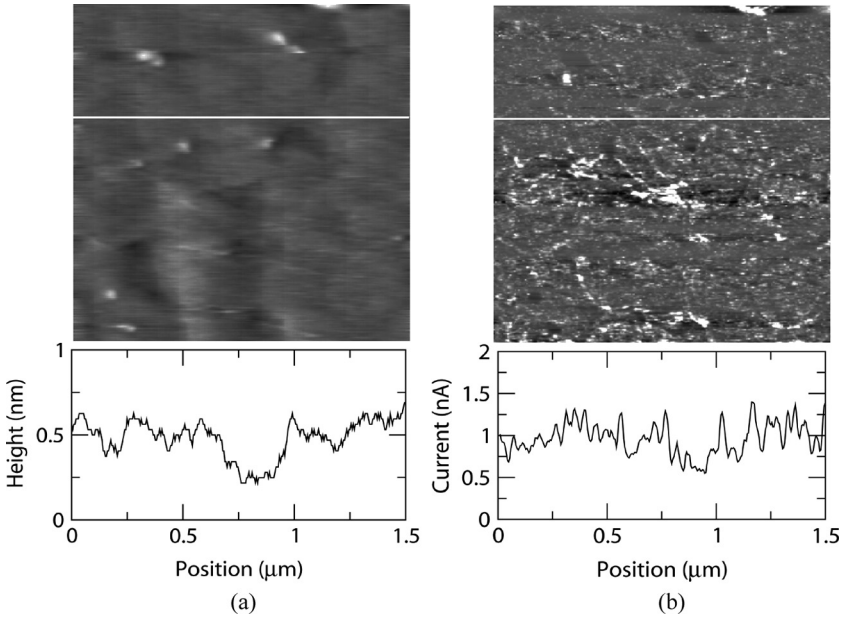

FIGURE 13 CS-AFM images of the monolayer film of PyTp on gold coated mica substrate at a sample bias of 2 V and a constant force of 4 nN: (a) Topography image showing the surface roughness. (b) Current image showing an average current of about 1 nA across the film. Reprinted with permission from *Phys. Rev. E* (http://link.aps.org/doi/10.1103/PhysRevE.78.021606), reference 20. Copyright 2008 by the American Physical Society.

tunneling current rapidly increased above a certain threshold voltage for both the films. For a given applied voltage, the value of current for PyTp film was significantly larger than that for PyTp-DNA complex

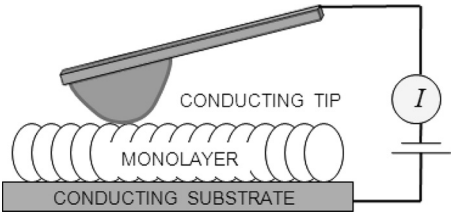

FIGURE 14 Metal-insulator-metal (M-I-M) junction drawn schematically for a conducting AFM tip in contact with a monolayer film deposited on a conducting substrate. Reprinted with permission from *Phys. Rev. E* (http://link.aps.org/doi/10.1103/PhysRevE.78.021606), reference 20. Copyright 2008 by the American Physical Society.

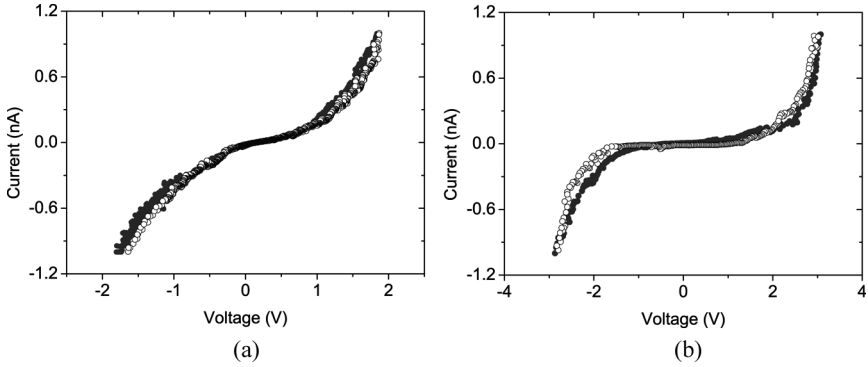

FIGURE 15 I-V curves obtained by CS-AFM on monolayer films of (a) PyTp and (b) PyTp-DNA complex, on gold coated mica substrates at a constant force of 4 nN. The solid circles represent forward voltage scan and the open circles represent reverse voltage scan. Reprinted with permission from *Phys. Rev. E* (http://link.aps.org/doi/10.1103/PhysRevE.78.021606), reference 20. Copyright 2008 by the American Physical Society.

film. With an applied bias of 1 Volt, the average electrical currents through PyTp and PyTp-DNA complex films were 0.2 nA and 0.05 nA, respectively.

The shape of the I-V curves strongly suggests a barrier for electron transport at the tip-sample interface. The barrier height at the interface is an important parameter for electron transfer across the interface. One can choose an appropriate model to describe the measured I-V curves and to determine the barrier height between the film and the metal substrate. We have considered two basic mechanisms for electron transport across a potential barrier; thermionic emission (Schottky emission) and electron tunneling. Thermionic emission can occur when the electrons have enough energy to pass over the potential barrier [25]. In the thermionic emission model for a M-I-M junction, the derivative dI/dV decreases with increasing current. In contrast, dI/dV increases with increasing current in the measured I-V curves. Therefore, the nature of the I-V curves suggests that the electron tunneling is the possible mechanism for electron transport in our system. For interpreting electron tunneling, Fowler-Nordheim (FN) model is widely used [26,27]. This model describes the electron tunneling from a metal's Fermi level over a barrier into an adjacent material.

For a M-I-M structure, the FN tunneling current is given by the following equation [28,29],

$$1 = \frac{A_{eff} q^3 E^2 m}{8\pi h \phi_b m^*} \exp\left[\frac{-8\pi\sqrt{2m^*}\phi_b^{-3/2}}{3hqE}\right] \quad (1)$$

where A_{eff} is the effective contact area, E is the applied electric field, ϕ_b is the contact barrier height, and q, m^*, m, and h are electron charge, effective mass of the electron, free electron mass, and Plank constant, respectively. If we assume $E = V/d$, where V is the applied voltage, and d is the separation between the two electrodes, then

$$I = AV^2 \exp\left(\frac{-B}{V}\right) \quad (2)$$

where

$$A = \frac{A_{eff} q^3 m}{8\pi h \phi_b d^2 m^*} \quad (3)$$

and

$$B = \frac{8\pi\sqrt{2m^*}\phi_b^{3/2} d}{3hq} = 6.83d\left(\frac{m^*}{m}\right)^{1/2}\phi_b^{3/2} \quad (4)$$

Here the units of B, d and ϕ_b are Volts, nm and eV, respectively. In our system, the separation between the two electrodes (d) is the distance between the probe and the gold substrate. Since the tip of the probe is located just at the surface of the LB film, d is same as the thickness of the film [27]. The interpretation of I-V curves in CS-AFM is straightforward as compared to STM studies due to the absence of an additional tunneling gap between the probe and sample surface.

Figures 16(a) and 17(a) show the log-linear representation of typical I-V curves for the pure and complex monolayer films, respectively. In recent reports by Casuso et al. and Beebe et al., a transition from direct tunneling to injection tunneling was observed [26,30]. The log-linear representation of the I-V curves in these two reports clearly indicated the transition between the two regimes. Further, it was highlighted by Casuso et al. that the presence of two different transport regimes made it possible to measure effective mass, m^* and effective area, A_{eff}. In our system, we did not observe an indication of a transition in the log-linear representation of the I-V characteristics. Hence, it was not possible for us to determine the effective electron mass, m^* and effective contact area, A_{eff}. Consequently, the A value (Eq. (3)) was not very useful in our case. We have used the B

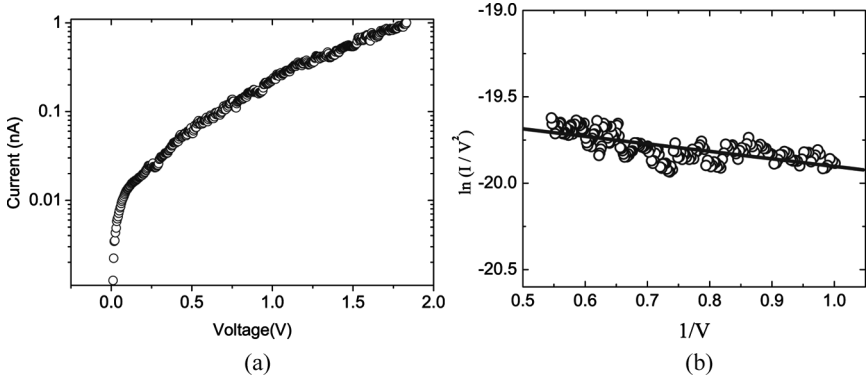

FIGURE 16 (a) Log-linear representation and (b) Fowler-Nordheim fitting to a typical I-V curve measured for the pure PyTp monolayer film at a constant force of 4 nN. Open circles represent the experimental data and solid line represents the fit. Reprinted with permission from *Phys. Rev. E* (http://link.aps.org/doi/10.1103/PhysRevE.78.021606), reference 20. Copyright 2008 by the American Physical Society.

value (Eq. (4)) for extracting the barrier heights for both the pure and complex monolayer films. For similar reasons, when it is difficult to calculate A_{eff}, researchers generally use B value to extract the barrier height [25].

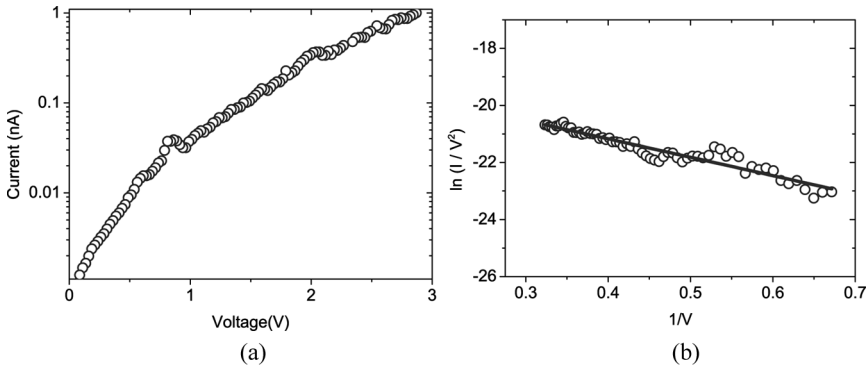

FIGURE 17 (a) Log-linear representation and (b) Fowler-Nordheim fitting to a typical I-V curve measured for the PyTp-DNA complex monolayer film at a constant force of 4 nN. Open circles represent the experimental data and solid line represents the fit. Reprinted with permission from *Phys. Rev. E* (http://link.aps.org/doi/10.1103/PhysRevE.78.021606), reference 20. Copyright 2008 by the American Physical Society.

We have fitted the I-V data for the pure and complex monolayer films with the FN model (Eq. (2)). Figures 16(b) and 17(b) show the FN plot of $\ln(I/V^2)$ against $1/V$ for the pure and complex films, respectively. The FN plot shows a straight line whose slope yields the B value. The open circles represent the experimental data points and the solid line represents the fit. We find that the I-V data for both the films fit well with this model. It is to be noted that FN is an approximation in the high voltage regime. Therefore, we have shown the fitting of our data for the high voltage regime only. At lower voltages, the system charging effect, thermal and Schottky effects become dominant which deprives us from extracting any meaningful information at that regime. On the basis of our analysis and within our experimental limits, we find FN to be a possible mechanism for electron transport in our system. We have obtained several I-V curves at different positions on the films and fitted them with the FN model. The average B values obtained from such measurements were 0.85 Volt for the pure film and 6.6 Volts for the complex film. The film thicknesses, as determined by scratching the films with AFM tip, were 2.2 nm for PyTp and 3.2 nm for PyTp-DNA complex. Using the average B values and the corresponding film thicknesses in equation 4, we have calculated the barrier heights, ϕ_b, to be $0.15(m/m^*)^{1/3}$ eV and $0.45(m/m^*)^{1/3}$ eV for the pure and complex films, respectively. In our system, the PyTp molecules in the LB films are arranged in columns. The FN fitting results suggest that for the pure film the barrier height may be as low as 0.15 eV. For PyTp-DNA complex system, we find that the presence of DNA leads to a larger barrier to electron transport. The higher barrier height is likely to be a direct consequence of change in packing of the molecules. The conformation of DNA molecule and the environment in which it is present have a crucial impact on its conductivity [13]. On the basis of our observations, we find that complexation with DNA makes the film more resistive.

IV. CONCLUSION

The novel cationic discotic mesogen, PyTp exhibited stable Langmuir monolayer which showed negligible hysteresis on expanding and compressing. As compared to the monolayers of non-ionic triphenylene derivatives reported so far, these cationic discogens showed higher limiting area per molecule due to the direct electrostatic repulsion between the molecules within the film. The presence of a cationic moiety in the PyTp molecule opens the scope for studying electrostatic interaction between such a molecule and a negatively charged species such as DNA at interfaces. We have shown the supramolecular

complexation between DNA and PyTp, at air-water interface. The PyTp-DNA complex was formed at the A-W interface primarily due to the electrostatic interaction between the pyridinium group of the triphenylene molecule and the phosphate group of DNA. The formation of the DNA complex has enhanced the transfer efficiency over several tens of layers. Employing a current sensing atomic force microscope, we have measured the nanoscale electrical conductivity of LB films of PyTp and PyTp-DNA complex. We find that the I-V curves fit well with the Fowler-Nordheim model indicating the electron tunneling to be a possible mechanism for electron transport. Further, analysis of the I-V curves based on the FN model yields the barrier height of PyTp-DNA complex film to be three times higher compared to that of the pure PyTp film.

REFERENCES

[1] Sergeyev, S., Pisula, W., & Geerts, Y. H. (2007). *Chem. Soc. Rev.*, *36*, 1902.
[2] Binnemans, K. (2005). *Chem. Rev.*, *105*, 4148.
[3] Josefowicz, J. Y., Maliszewskyj, N. C., Idziak, S. H. J., Heiney, P. A., McCauley, J. P., & Smith, A. B. (1993). *Science*, *260*, 323.
[4] Schwartz, D. K. (1997). *Surface Science Reports*, *27*, 241.
[5] Bhaumik, A., Ramakanth, M., Brar, L. K., Raychaudhuri, A. K., Rondelez, F., & Chatterji, D. (2004). *Langmuir*, *20*, 5891.
[6] Radler, J. O., Koltover, I., Salditt, T., & Safinya, C. R. (1997). *Science*, *275*, 810.
[7] Yoon, T.-Y., Jeong, C., Lee, S.-W., Kim, J. H., Cho, M. C., Kim, S.-J., Kim, M. W., & Lee, S.-D. (2006). *Nature Materials*, *5*, 281.
[8] Frances, M. P. W., Dorothy, L. R., & Marcel, B. B. (1996). *Biochemistry*, *35*, 5756.
[9] Sastry, M., Ramakrishnan, V., Pattarkine, M., Gole, A., & Ganesh, K. N. (2000). *Langmuir*, *16*, 9142.
[10] Sukhorukov, G. B., Montrel, M. M., Petrov, A. I., Shabarchina, L. I., & Sukhorukov, B. I. (1996). *Biosens. Bioelectron.*, *11*, 913.
[11] Cui, L., Miao, J., & Zhu, L. (2006). *Macromolecules*, *39*, 2536.
[12] Na, J.-H., Kim, J., Choi, W., Bae, J.-H., & Lee, S.-D. (2007). *Mol. Cryst. Liq. Cryst.*, *476*, 125.
[13] Endres, R. G., Cox, D. L., & Singh, R. R. P. (2004). *Rev. Mod. Phys.*, *76*, 195.
[14] Nazin, G. V., Qiu, X. H., & Ho, W. (2003). *Science*, *302*, 77.
[15] Guisinger, N. P., Yoder, N. L., & Hersam, M. C. (2005). *Proc. Natl. Acad. Sci. U.S.A*, *102*, 8838.
[16] Han, D.-H., Kim, J.-W., & Park, S.-M. (2006). *J. Phys. Chem. B*, *110*, 14874.
[17] Nayak, A., Suresh, K. A., Pal, S. K., & Kumar, S. (2007). *J. Phys. Chem. B*, *111*, 11157.
[18] Nayak, A. & Suresh, K. A. (2008). *J. Phys. Chem. B*, *112*, 2930.
[19] Pisula, W., Menon, A., Stepputat, M., Lieberwirth, I., Kolb, U., Tracz, A., Sirringhaus, H., Pakula, T., & Mullen, K. (2005). *Adv. Mater.*, *17*, 684.
[20] Nayak, A. & Suresh, K. A. (2008). *Phys. Rev. E*, *78*, 021606.
[21] Kumar, S. & Pal, S. K. (2005). *Tetrahedron Lett.*, *46*, 4127.
[22] Broniatowski, M., Sandez Macho, I., Minones, J. Jr., & Dynarowicz-Latka, P. (2004). *J. Phys. Chem. B*, *108*, 13403.

[23] Davies, J. T. & Rideal, E. K. (1963). *Interfacial Phenomena*, Academic Press: New York.
[24] Okahata, Y., Kobayashi, T., & Tanaka, K. (1996). *Langmuir*, *12*, 1326.
[25] Xu, D., Watt, G. D., Harb, J. N., & Davis, R. C. (2005). *Nano Lett.*, *5*, 571.
[26] Casuso, I., Fumagalli, L., Samitier, J., Padros, E., Reggiani, L., Akimov, V., & Gomila, G. (2007). *Phys. Rev. E*, *76*, 041919.
[27] Yano, K. *et al*. (1996). *Appl. Phys. Lett.*, *68*, 188.
[28] Simmons, J. G. (1963). *J. Appl. Phys.*, *34*, 1793.
[29] Lenzlinger, M. & Snow, E. H. (1969). *J. Appl. Phys.*, *40*, 278.
[30] Beebe, J. M., Kim, B. S., Gadzuk, J. W., Frisbie, C. D., & Kushmerick, J. G. (2006). *Phys. Rev. Lett.*, *97*, 026801.